Available online at www.sciencedirect.com
ScienceDirect
International Journal of Heat and Mass Transfer 50 (2007) 1569–1576
International Journal of HEAT and MASS TRANSFER
www.elsevier.com/locate/ijhmt

Radiative heat transfer in preforms for microstructured optical fibres

S.-C. Xue [a,d,*], L. Poladian [b], G.W. Barton [c], M.C.J. Large [d]

[a] School of Aerospace, Mechanical and Mechatronic Engineering, The University of Sydney, NSW 2006, Australia
[b] School of Mathematics and Statistics, The University of Sydney, NSW 2006, Australia
[c] School of Chemical and Biomolecular Engineering, The University of Sydney, NSW 2006, Australia
[d] Optical Fibre Technology Centre, The University of Sydney, NSW 2006, Australia

Received 15 May 2006; received in revised form 25 August 2006
Available online 25 October 2006

Abstract

Air inclusions in any preform for microstructured optical fibres can greatly reduce conductive heat transfer. Modelling the heat transfer therefore requires that radiation be properly included. In this paper we use the Rosseland approximation to consider radiative heat transfer within the matrix material and present a method of including radiative heat transfer across the air inclusions for the first time. We apply the thermal model to the transient heating process of a silica preform with a hole structure that restricts conduction. The resultant heat transfer model yields realistic heating times.

Keywords: Fibre fabrication; Holey fibres; Microstructured optical fibres (MOFs); Photonic crystal fibres (PCFs); Numerical modelling; Thermal radiation heat transfer

1. Introduction

Microstructured optical fibres (MOFs), also known as photonic crystal fibres or holey fibres, achieve their optical properties through a pattern of tiny holes that run the entire length of the fibre [1]. Unlike conventional optical fibres, which rely on refractive index contrasts produced by chemical doping or the use of more than one material, MOFs are usually made from a single material, either silica [1,2] or polymer [3]. The development of MOFs has aroused enormous interest because of their ability to produce a wide range of optical effects. Some of these, such as photonic bandgap guidance, which allows light to be guided in air, cannot be obtained using conventional fibres. In other cases, the use of a microstructure allows unusually strong effects to be produced, affecting for example the fibre's polarisation or dispersion properties.

The wide range of optical properties in such fibres is obtained by the use of different microstructures, and in some MOFs the optical performance is critically dependent on the exact geometry of particular features in the design. Fig. 1 shows an example of a typical MOF.

Like other optical fibres, MOFs are produced from a shorter, fatter version of the final fibre called a 'preform'. The preform is drawn to fibre by heating and applying tension. This process has been described elsewhere [4,5] and usually involves one or two draw stages to obtain fibre structures of the required size. In silica, the preforms are usually 2–3 cm in diameter, while in polymer they can be up to 8 cm in diameter. Fibre diameters typically fall in the range 100–500 μm, with silica MOFs often being drawn to a 'standard' 125 μm.

The relationship between the hole structure and the optical properties means that the fabrication process poses challenges, as holes can change both their size and shape during the draw process. Initially, the complexity of this problem meant that it was approached empirically. More recent work however [6–8] has begun to give insights into the underlying mechanisms of hole deformation, and has

* Corresponding author. Address: School of Aerospace, Mechanical and Mechatronic Engineering, The University of Sydney, NSW 2006, Australia. Tel.: +61 2 93517151; fax: +61 2 93527060.
E-mail address: shicheng@aeromech.usyd.edu.au (S.-C. Xue).

0017-9310/$ - see front matter © 2006 Elsevier Ltd. All rights reserved.
doi:10.1016/j.ijheatmasstransfer.2006.08.027

Nomenclature

c	speed of light in a vacuum (2.9×10^8 m/s)
c_p	specific thermal capacity (J/kg K)
ds	length of a differential segment
$d\varphi$	azimuthal angle
F	radiative view factor
h	Planck's constant (6.626×10^{-34} J s)
H	incident radiation (W/m^2)
k_B	Boltzmann's constant (1.3807×10^{-23} J/K)
J	total radiated power (or radiosity) (W/m^2)
n	refractive index
n	normal unit vector to a surface
N	number of surfaces in enclosure
Q	heat flux at a surface (W/m^2)
q	radiative heat flux vector within the matrix material (W/m^2)
r	radial coordinate
R	radius (m)
t	time (s)
t_s	time when the centre of a preform reaches T_s
t_e	time when the centre of a preform reaches 'near equilibrium'
T	temperature (K)
T_s	softening temperature of the preform material (K)
x, y	coordinates

Greek symbols

α	absorption coefficient (m^{-1})
α_m	Rosseland mean absorption coefficient (m^{-1})
δ	optical thickness
ε	hemispherical emissivity
ε_e	effective emissivity
κ_c	thermal conductivity (W/m K)
κ_r	radiative 'conductivity' (W/m K)
λ	free space wavelength (μm)
ρ	reflectivity
ρ_o	density (kg/m^3)
σ_0	Stefan–Boltzmann constant (5.68×10^{-8} W/m^{2}K^4)

Subscripts

c	quality related to conductive heat transfer
con	quality related to convective heat transfer
h	hole
i, j	surface i or j
$i-j$	from surface i to surface j
m	mean value
max	maximum value
min	minimum value
p	preform surface
w	furnace wall
rad or r	quality related to radiative heat transfer
λ	spectrally (wavelength) dependent

shown excellent qualitative agreement with experiment. The ultimate aim of the present research is to be able to 'reverse engineer' the preform and its drawing conditions so as to produce the desired microstructure in the fibre. This however requires a more quantitative understanding of the heat transfer processes, as the temperature profile in the preform also determines the profile of key rheological parameters such as viscosity.

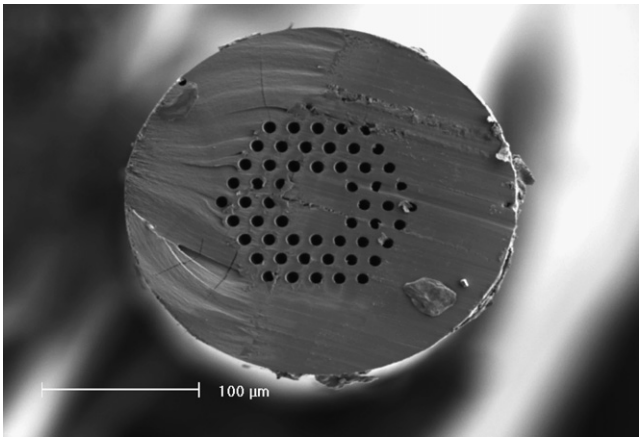

Fig. 1. Cross-section of a typical MOF (Image courtesy of Richard Lwin).

Heat transfer in the transient heating process of MOF preforms for drawing optical fibres is complex because it involves structures made from semitransparent materials heated at elevated temperatures. Like many engineering problems, combined conduction, convection, radiation heat transfer [9] has to be considered. To solve the coupled heat transfer problems, great efforts have been made in developing sophistic numerical methods, including finite volume methods [10–12], finite element methods [13], boundary element method [14], and discrete transfer method [15].

There have been previous studies of heat transfer in MOF preforms and drawing optical fibres. In considering the heat transfer inside preforms or solid fibres, the matrix material was usually assumed to be optically thick [16] so that the Rosseland or diffusion approximation can be used [17–21]. In studying the heat transfer in MOF preforms, Lyytikäinen et al. [20] considered radiative transfer within the matrix material while later work [22] looked at the impact of hole structure on the time dependent heating behaviour of a polymer preform. Deflandre [23] investigated thermal effects on the periodicity and hole shape

under steady-state drawing conditions. However, in all of these studies, either a constant absorption coefficient or a mean absorption coefficient evaluated at a particular temperature was used over the entire temperature range in the transient heating process, and none of these studies considered radiative heat transfer across the holes. As thermal radiation is the principal heat transfer mechanism within the holes by the fact that no conduction exists in the air inside, and neglecting it might be expected to produce substantially inaccurate results.

In this work we propose a method for evaluating the radiative heat transfer across the holes located at arbitrary positions in a microstructured preform, and improve the radiation model used within the optically thick matrix material. We then apply this model to the transient heating process of a silica preform whose hole structure is such as to severely limit thermal conduction, and show that including radiative heat transfer gives realistic heating times.

2. Thermal modelling

In the heating and drawing process of MOFs, a cylindrical preform (initially at room temperature) of initial radius R_p is fed into a cylindrical furnace at a relatively slow, constant speed, and heated to a temperature above the softening point T_s of the material. Fibres are continuously drawn from the end of the softened preform by applying an appropriate level of tension. In this work we consider only the initial transient heating process to the draw temperature, before the fibre drawing begins. This process can be regarded as the thermal transport system between two infinitely long concentric cylinders (the preform and furnace), with the preform having an arrangement of longitudinal holes. The transient energy equation for this simplified system is thus:

$$\rho_0 c_p \frac{\partial T}{\partial t} = -\nabla \cdot (-\kappa_c \nabla T + \mathbf{q}) \tag{1}$$

where T is temperature, t is time, ρ_0 is the mass density, c_p is specific thermal capacity, κ_c is thermal conductivity and $\mathbf{q}$ denotes the radiative heat flux. The boundary conditions are $\frac{\partial T}{\partial r} = 0$ at $r = 0$, and $\kappa_c \mathbf{n} \cdot \nabla T = Q_{con} + Q_{rad}$ on the surfaces of the preform and the holes involved. Here, $\mathbf{n}$ is the normal vector of the surfaces, and Q_{con} and Q_{rad} are respectively the convective and radiative heat fluxes.

In the following sub-sections, we will consider separately the effect of radiation in both the matrix material and across the preform holes. In both cases, we find ways express the radiation in terms of the temperature profiles.

2.1. Radiative heat transfer within the matrix material

The effect of radiation incident on the preform depends on the transparency of the material. Clearly, if the material is completely transparent it will pass through the material and there will be no radiative heat transfer. Similarly, if the material is completely opaque, the radiation will be absorbed at the surface and the subsequent heat transfer into the preform will be by conduction alone. An important intermediate case is therefore when the material is 'optically thick' allowing for the short-range transmission of thermal radiation, that is, when the mean optical thickness of the matrix material $\delta_m = 2\alpha_m R_p \gg 1$. Here, α_m is the mean absorption coefficient of the preform material. In this case, as addressed by Sparrow and Cess [24], the photon mean free path (i.e., $1/\alpha_m$) is much smaller than the characteristic dimension (i.e., R_p). As a result, every element of the matrix material is directly affected only by it neighbours, and the radiation transfer within the matrix material becomes a diffusion process, and one can use the Rosseland diffusion equation [16] rather than solving the radiative transfer equations (RTE) to obtain the heat flux due to radiation. In this approach, one begins with the formula of the spectral distribution e_λ for black-body radiation into a medium with a constant refractive index n. This can be written in the factorised form

$$e_\lambda \, d\zeta = (n^2 \sigma_0 T^4) \left(\frac{15}{\pi^4} \frac{\zeta^3}{e^\zeta - 1} \right) d\zeta \tag{2}$$

where

$$\zeta = \frac{h\nu}{k_B T} = \frac{hc}{\lambda k_B T} \tag{3}$$

is the dimensionless ratio of photon energy to thermal energy. In Eq. (2) the first factor contains the important physical quantities while the second is normalised such that its integral over the entire spectrum is unity. The associated Rosseland equation

$$d\mathbf{q} = -\frac{4}{3\alpha_\lambda} \nabla (e_\lambda \, d\zeta) \tag{4}$$

shows that the heat flux $\mathbf{q}$ per unit spectral range $d\zeta$ is proportional to the gradient of the spectral distribution and inversely proportional to the absorption α_λ. In a homogeneous, unstructured material the only source of spatial variation is the temperature, so one can rewrite the Rosseland equation as

$$d\mathbf{q} = -\frac{4}{3\alpha_\lambda} \nabla T \frac{\partial}{\partial T} (e_\lambda \, d\zeta) \tag{5}$$

The total heat flux is then obtained by integrating over the relevant parts of the spectrum:

$$\mathbf{q} = -\frac{4}{3} \nabla T \frac{\partial}{\partial T} \int \frac{e_\lambda \, d\zeta}{\alpha_\lambda} = -\kappa_r \nabla T \tag{6}$$

Thus, we obtain the most important result of the Rosseland approximation: the radiative heat flux behaves like thermal conduction and is proportional to the local temperature gradient. An effective radiative 'conductivity' may then be defined as

$$\kappa_r = \frac{4}{3} \frac{\partial}{\partial T} \int \frac{e_\lambda \, d\zeta}{\alpha_\lambda} \tag{7}$$

In general, the integral in Eq. (7) must be evaluated numerically. One special case that can be solved analytically is

when the absorption is a constant over the entire spectral range and we can exploit the normalisation of Eq. (2) to obtain

$$\kappa_r = \frac{4}{3\alpha}\frac{\partial}{\partial T}\int e_\lambda \, d\zeta = \frac{16}{3\alpha} n^2 \sigma_0 T^3 \tag{8}$$

This reveals the familiar cubic dependence on temperature.

For many materials radiative absorption takes place in distinct spectral bands with different levels of absorption in each. The previous integral must therefore be calculated separately for each band. This means that the effective Rosseland conductivity will have a more complicated form than that shown in Eq. (7)

$$\kappa_r = \frac{4}{3}\sum_i \frac{\partial}{\partial T}\int_{\text{band},i} \frac{e_\lambda \, d\zeta}{\alpha_\lambda} = \frac{16}{3\alpha_m} n^2 \sigma_0 T^3 \tag{9}$$

where α_m is the Rosseland mean absorption coefficient. From Eq. (9), α_m can be cast as

$$\frac{1}{\alpha_m} = \frac{1}{4n^2\sigma_0 T^3}\sum_i \frac{\partial}{\partial T}\int_{\text{band},i} \frac{e_\lambda \, d\zeta}{\alpha_\lambda} \tag{10}$$

or after some algebra as

$$\frac{1}{\alpha_m} = \frac{15}{4\pi^4}\sum_i \int_{\text{band},i} \frac{\zeta^4 e^\zeta}{(e^\zeta - 1)^2}\frac{d\zeta}{\alpha_\lambda}. \tag{11}$$

This approach is sometimes referred to in the literature as the "gray bands" model. Unfortunately these integrals cannot be evaluated in closed form, and a mean absorption coefficient must be computed numerically. (See Eq. (22) below for the actual parameters used in our simulations for silica preforms.)

The gray bands approximation is not, however, the only modification required to apply the Rosseland approximation. From Eqs. (3) and (11), clearly, α_m is a function of wavelength- temperature product. As the temperature of a black-body increases, the maximum hemispherical radiation emissive power shifts to shorter wavelengths, so that α_m must be evaluated numerically for each temperature in the temperature range determined by the intensity of black-body hemispherical emissive power. Accounting for this is particularly significant in heating silica preforms because at the draw temperature (2000 K) the emission peak falls in a wavelength region where silica is highly transparent. At this temperature radiation clearly does not contribute to the heat transfer, and the Rosseland approximation is invalid.

The point at which the Rosseland approximation becomes inappropriate can be estimated using Wien's displacement law, which relates the peak of the (free-space) wavelength to the temperature:

$$\lambda_{\text{peak}} T = 2898 \ \mu\text{m K} \tag{12}$$

More than 75% of the emissive power is concentrated in the following range of wavelength-temperature products (see, for example, Figs. 2–7 in [16]):

$$1448 \ \mu\text{m K} \leqslant \lambda T \leqslant 6149 \ \mu\text{m K} \tag{13}$$

If $\lambda_{\min}$ is the minimum wavelength and $\lambda_{\max}$ is the minimum wavelength for which the preform material can be considered optically thick, then temperature range over which the Rosseland approximation appropriate is

$$\frac{1448 \ \mu\text{m K}}{\lambda_{\max}} \leqslant T \leqslant \frac{6149 \ \mu\text{m K}}{\lambda_{\min}} \tag{14}$$

Therefore, for a given wavelength band, the working range of the Rosseland model is restricted in the range given in Eq. (14) (Note, if the value below the room temperature, the room temperature 298 K will be used). As a result, a temperature-dependent, thus, time-dependent, mean absorption coefficient is numerically evaluated based on Eq. (11) point-wisely inside material. Outside this temperature range, it is assumed that the matrix material is either transparent (at a high temperature and low wavelength) or opaque (at a high wavelength $\alpha_m = \infty$), and accordingly, no radiation is considered inside the matrix material.

2.2. Radiative heat transfer across holes within the preform

During the transient heating process of a microstructured preform, the temperature around a hole surface varies with time and position, and so radiative heat transfer is expected between different parts of the hole surface. Simply imposing a zero heat flux condition on the hole surface [20,22,23] is a poor assumption that becomes worse as the number of holes increases, or their spacing decreases.

Using the net-radiation method for an enclosure [16], it is possible to derive an expression for the relationship between the localised heat flux due to radiative heat transfer and the temperature around the perimeter of an off-axis air-hole. For simplicity, we consider only circular holes in this work, although the method can clearly be generalised for holes of any shape.

With the net-radiation method, the perimeter of each off-axial hole is divided into N differential segments of length $ds_i = R_h d\varphi_i$ $(1 \leqslant i \leqslant N)$ where φ is the azimuthal angle around the hole and R_h is the radius of the hole, as shown in Fig. 2. Each segment is sufficiently short that it can be treated as an isothermal straight line. Assume each of the segments be a gray, diffuse radiator with a constant hemispherical total emissivity ε_i, absorption α_i and reflectivity ρ_i related by $\varepsilon_i = \alpha_i = 1 - \rho_i$. The heat loss Q at the surface of the ith segment is the difference between thermal emission and absorption

$$Q_i = \varepsilon_i \sigma_0 T_i^4 - \alpha_i H_i \quad 1 \leqslant i \leqslant N. \tag{15}$$

Similarly, the radiated power, or radiosity J, is the sum of the emission and reflection

$$J_i = \varepsilon_j \sigma_0 T_i^4 + \rho_i H_i \tag{16}$$

Here T_i is the local temperature and H_i is radiation incident on the surface from all the other segments around the hole:

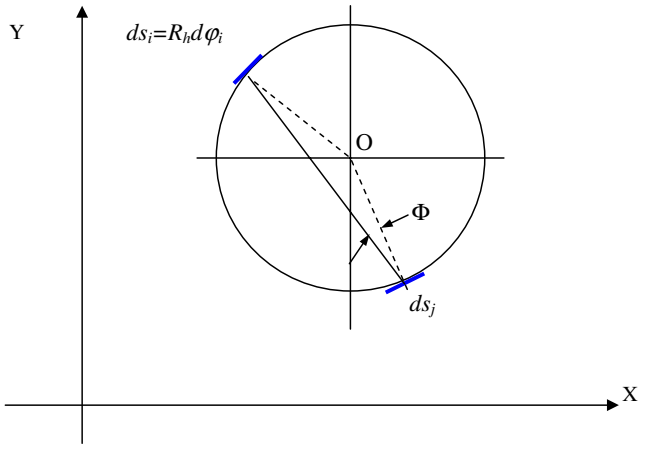

Fig. 2. The circumference of the hole is divided into N segments of length ds each of which emit, as well as reflecting and absorbing radiation from the other segments. Calculating the interaction between the segments requires a pair-wise view factor. Here, the solid line shows the line of sight between segments i and j while the dashed lines show the normal of each segment. The angle between them is $\Phi = \frac{\pi}{2} - \frac{\varphi_i - \varphi_j}{2}$.

$$H_i = \sum_{j=1}^{N} J_j F_{i-j} \tag{17}$$

where F_{i-j} is the view factor and the subscript i denotes the emitting element while j denotes the incident element.

Combining Eqs. (15) and (17) yields

$$Q_i = \varepsilon_i \sum_{j=1}^{N} (\sigma_0 T_i^4 - J_j) F_{i-j} \tag{18}$$

Thus, to determine the net heat flux Q_i it is only necessary to determine J_i

$$J_i = \varepsilon_i \sigma_0 T_i^4 + (1-\varepsilon_i) \sum_{j=1}^{N} J_j F_{i-j} \quad 1 \leqslant i \leqslant N \tag{19}$$

The view factor between two segments at angular positions φ_i and φ_j is related to the projection of the normal to the segment along the line of sight between the segments (see Fig. 2). Some simple trigonometry gives

$$\cos(\Phi) = \sin\left(\frac{\varphi_i - \varphi_j}{2}\right) \tag{20}$$

It is easy to see that for diametrically opposite segments this factor is unity and decreases as the two segments become relatively inclined. The full view factor F_{i-j} is obtained by considering two infinitely long strips having parallel generating lines which introduces an additional factor of a half (see [16] for example)

$$F_{i-j} = \frac{1}{2} \sin\left(\frac{\varphi_i - \varphi_j}{2}\right) \tag{21}$$

With known view factors and temperatures, Eq. (19) can be readily solved numerically by matrix inversion and only needs to be inverted once. It is also worth noting that the size of the hole does not explicitly appear in the relationship.

3. Numerical analysis

The importance of air holes within a preform on its transient heating depends on the structure used. Although air acts as a barrier to conduction, the degree to which it alters the radial temperature profile and changes heating times is often not intuitive. Indeed even without radiative transfer across the holes, preforms with very high air fractions may be heated more rapidly than solid preforms due to the reduced amount of material present [22], particularly for those hole structures where there are no hole-rings formed.

In order to test our heat transfer model, we chose a symmetric 8-hole structure where the holes form an almost complete 'air ring' (see Fig. 3 – only one quarter of the symmetric cross-section is shown). This structure greatly reduces conductive heat transfer into the central part of the preform, and therefore would be expected to provide a graphic demonstration of the impact of radiative heating across the holes.

The preform radius used was $R_p = 12.5$ mm, with a hole radius $R_h = 2.2$ mm. The holes were placed symmetrically at a radial distance of 6 mm. We used silica as the matrix material, as it is the most commonly used material for MOFs. The heating conditions and material properties used are given in Table 1. The simulations were carried out using a commercial computational fluid dynamics package, Fluent [25].

As described in Section 2.1, the absorption of silica varies with wavelength and can be divided into bands over which the absorption is taken to be constant. The band model given by Myers [19] at 298 K defines the absorption coefficients as follows:

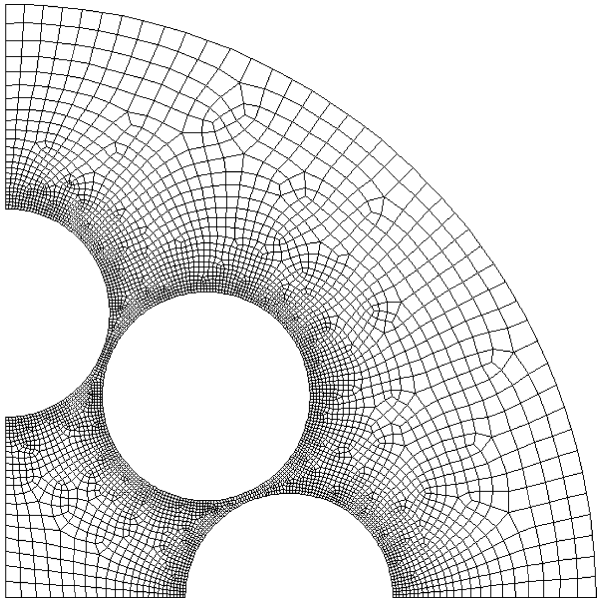

Fig. 3. The computational domain and mesh structure used in the transient heat transfer modelling.

Table 1
Material properties and heating conditions used in the numerical simulations

Parameter	Silica value		Units
ρ_0	2200		kg/m^3
κ_c	2.68		W/m K
c_p	1345		J/kg K
T_s	1900		K
T_w	2000		K
ε_e	Eq. (24)		–
ε_p	Eq. (25)		–
n	1.42		–
α_m	Eqs. (11) and (22)	298 K $\leqslant T \leqslant$ 1443 K	1/m
	∞	$T >$ 1443 K	

$$\alpha_\lambda = \begin{cases} 0 & \lambda < 3\ \mu\text{m} \\ 400\ \text{m}^{-1} & 3\ \mu\text{m} \leqslant \lambda \leqslant 4.8\ \mu\text{m} \\ 15,000\ \text{m}^{-1} & 4.8\ \mu\text{m} < \lambda \leqslant 8\ \mu\text{m} \\ 0 & \lambda > 8\ \mu\text{m} \end{cases} \tag{22}$$

The temperature range in which the silica preform is optically thick is $298 \leqslant T\,(\text{K}) \leqslant 1443$ [see Eq. (14)], which has been clearly demonstrated in Fig. 4 where the calculated temperature-dependent mean absorption coefficient α_m, the effective radiative 'conductivity' κ_r (see Eq. (9)) and the mean optical thickness δ_m of the silica preform in the temperature range are depicted. As seen, $\delta_m \gg 1$, and κ_r is roughly proportional to the temperature in this temperature range, but compared to the material thermal conductivity κ_c, it is relatively smaller, particularly at a lower temperature, which indicates that radiative heat transfer inside the matrix material is not the dominant mode in the transient heating process of microstructured silica preform.

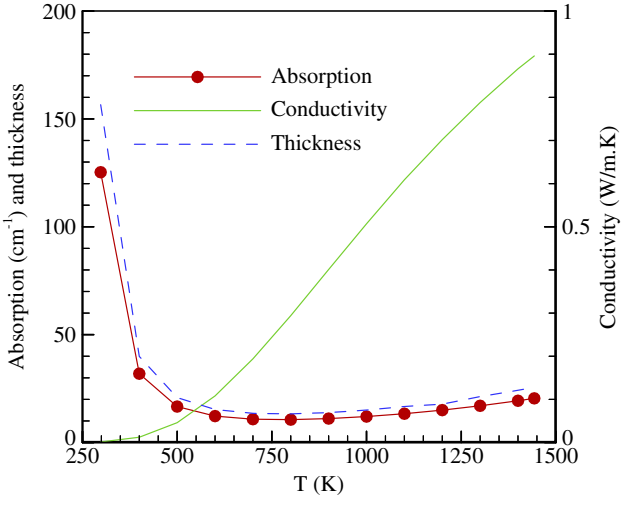

Fig. 4. Calculated temperature-dependent mean absorption coefficient α_m, (solid line with symbols), the effective radiative 'conductivity' κ_r (solid line) and the mean optical thickness δ_m (dashed line) of the silica preform of radius $R_p = 12.5$ mm in the temperature range where it is optically thick.

The external heat flux due to radiative transfer is

$$Q_{rad} = -\varepsilon_e \sigma_0 [T^4 - T_w^4] \tag{23}$$

where the effective emissivity ε_e is given by Christiansen's equation

$$\varepsilon_e = \frac{1}{\frac{1}{\varepsilon_p} + \left(\frac{R_p}{R_w}\right)^2 \left(\frac{1}{\varepsilon_w} - 1\right)} \tag{24}$$

The furnace wall is assumed to be gray and diffuse with a hemispherical total emissivity ε_w of 0.75 [16] at a representative temperature of 2000 K. Over the wavelength range $0.1\ \mu\text{m} < \lambda < 100\ \mu\text{m}$, silica is treated as a diffuse spectral surface, where the value of the hemispherical spectral emissivity ε_p for a glass cylinder has been estimated by Sayles and Caswell [26] as

$$\varepsilon_p = 0.885(1 - e^{-\delta_\lambda}) \tag{25}$$

where $\delta_\lambda = 2\alpha_\lambda R_p$ is the spectrally dependent optical thickness of the silica preform.

Only one quarter of the cross-section was required due to symmetry, and the computational domain (see Fig. 3) was discretised as 4650 quadrilateral control volumes. To ensure each cell face is nearly straight for accurate calculations of the view factors, very fine meshes were used around the holes (with a minimum dimensionless size of 0.0018 relative to the hole perimeter).

In order to quantitatively compare various preform heating scenarios, we defined the following several parameters. The softening time, t_s, is the time when the centre of the preform reaches the softening temperature of silica T_s. The time taken to reach near equilibrium, t_e, is defined here to be when the centre temperature is within 0.5% of the external driving temperature. Finally, the percentage radial temperature difference across the preform at t_s is quantified by

$$\Delta T = \left(\frac{T_{p,max} - T_s}{T_s}\right) \times 100\% \tag{26}$$

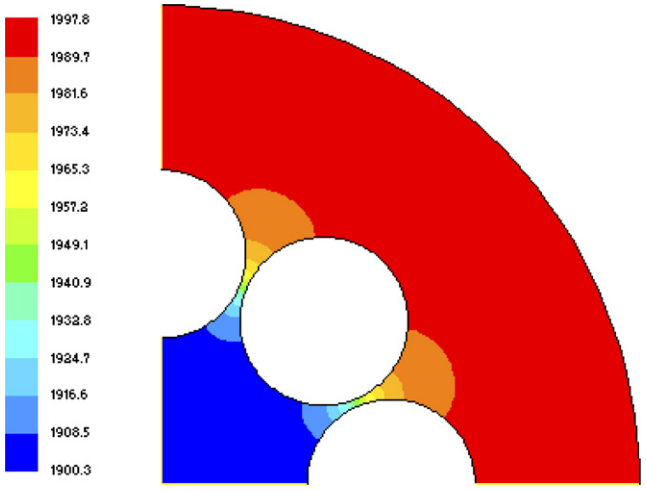

Fig. 5. The temperature profile (contour in K) without radiative heat transfer across the hole structure. The profile is shown at time $t_s = 4$ min.

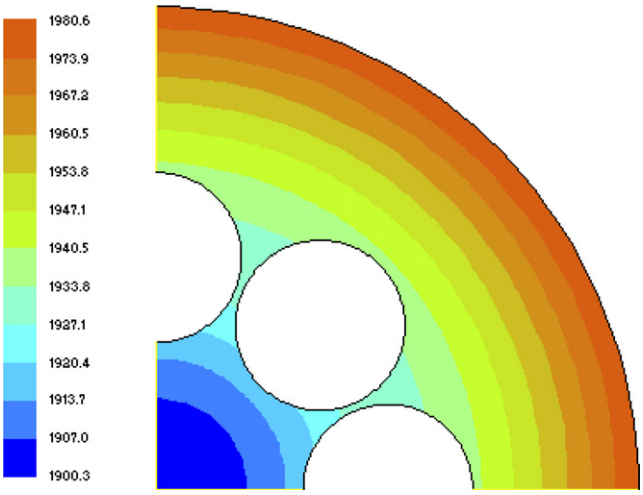

Fig. 6. The temperature profile (contour in K) with radiative heat transfer across the hole structure. The profile is shown at time $t_s = 1.48$ min.

Note that $T_{p,max}$ is the maximum temperature of the preform surface at t_s.

Figs. 5 and 6 show temperature profiles (contours in K) at t_s, for cases with and without the inclusion of radiative transfer across the holes. In both cases, conduction and radiative transfer (the latter included via the Rosseland approximation) through the silica matrix have been included.

Fig. 5 shows that the air holes present a significant barrier to conductive heat transfer with the thinnest points in the bridges effectively acting as point sources of heat. By contrast, when radiative transfer across the holes is included (Fig. 6), the temperature contours indicate an insignificant perturbation due to the presence of the holes.

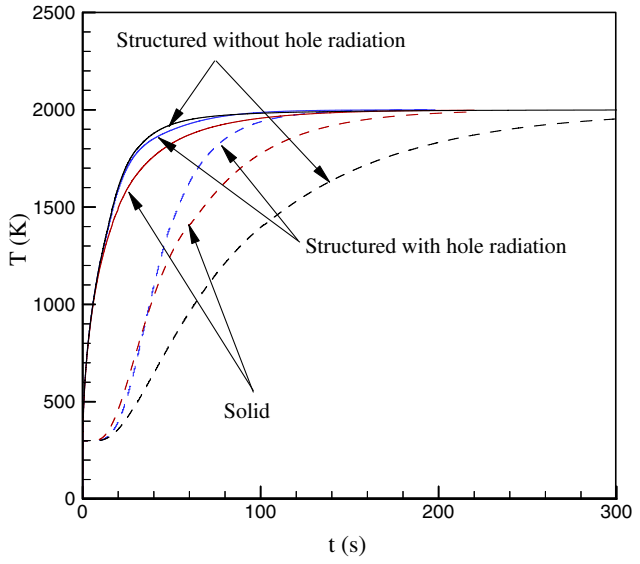

Fig. 7. The evolution with time of the maximum temperature on the preform surface (solid lines) and the temperature at the preform centre (dashed lines) for a solid preform and a 8-hole ring preform with and without radiative heat transfer across the holes.

Table 2
Heating efficiency and temperature uniformity in solid and structured preforms

Preform	t_s	t_e	$\Delta T\%$
Solid	1	1.68	4.27
8-hole ring structure (*no radiation across holes*)	1.82	3.26	5.15
8-hole ring structure (*radiation across holes*)	0.67	1.08	4.24

Times have been scaled relative to t_s for the solid preform.

When the centre of the preform reaches the silica softening point T_s, the difference in temperature between the surface and centre is some 17 K lower than when radiative transfer across the holes is not included.

The evolution with time of the maximum temperature at the preform surface and at the preform centre is shown in Fig. 7 where, for reference, the results for a solid preform of the same dimensions have been included. The surface temperatures in the two structured cases increase somewhat more rapidly than for the solid preform case, a result that is simply due to there being less material to heat. As expected, the centre of the structured preform with no radiative transfer across the holes heats most slowly and exhibits the largest radial temperature difference. When radiation across the holes is included, the preform heats more quickly than the solid preform, again due to the reduced amount of material present. The uniformity of heating in this latter case, is marginally better than for a solid preform.

A quantitative comparison of all three cases is shown in Table 2 where all the characterizing times have been scaled by t_s of the corresponding solid (unstructured) preform.

4. Conclusions

The results clearly demonstrate the need to include thermal radiation across the hole structure when modelling heat transfer within an MOF preform. In addition they indicate that at high air fractions heating is faster and more uniform than for a corresponding solid preforms despite the reduced transfer area for conductive heat transfer. This latter result is particularly important in the case of photonic band-gap fibres which require a very high (at least 90%) air fraction. While thermal radiation is the norm when heating preforms for silica MOFs, the authors are unaware of any modelling work that includes radiative transfer across the hole structure. Certainly this heat transfer mode has not been considered when modelling the heating of non-silica preforms. Our results would indicate that this is a serious omission in such transient thermal modelling.

Preform heating is very rapid in the cases we considered, with thermal equilibrium being essentially reached in less than 4 min. It is worth noting that in practice much longer heating times (of the order 20–30 min) are used, with a ramped furnace temperature to reduce thermal shock and minimise the risk of the preform shattering. An additional

influence here is that silica draw towers continuously flush the furnace with inert gas (at room temperature) to prevent oxidation of the graphite furnace elements and remove carbonaceous debris [27]. This forced convection has not been included in our thermal model. The surface cooling that it causes would have the effect of increasing the heating times and reducing the radial temperature gradient. The impact of external convective heat transfer on the heating (and drawing to fibre) of polymer preforms has been considered previously [6,7].

Experimental confirmation of this thermal modelling is problematic for silica preforms due to the high temperatures used. While radiative heat transfer is less important in polymer preforms because of the lower operating temperature, it is far easier to obtain transient heating data for such systems using a set of embedded thermocouples. Experimental and modelling results from the transient heating of polymer preforms will be compared in a later paper.

References

[1] J.C. Knight, T.A. Birks, R.F. Russsell, D.M. Atkins, All silica single-mode optical fiber with photonic crystal cladding, Opt. Lett. 21 (19) (1996) 1547–1549.

[2] P.St.J. Russell, Photonic crystal fibre, Science 299 (2003) 358–362.

[3] M.A. van Eijkelenborg, M.C.J. Large, A. Argyros, J. Zagari, S. Manos, N.A. Issa, I. Bassett, S. Fleming, R.C. McPhedran, C.M. de Sterke, N.A.P. Nicorovici, Microstructured polymer optical fibre, Opt. Exp. 9 (7) (2001) 319–327.

[4] J.C. Knight et al., "Holey" Silica Fibers, in: V. Markel, T. George (Eds.), Optics of Nanostructured Materials, John Wiley and Sons, 2001.

[5] G. Barton, M.A. van Eijkelenborg, G. Henry, M.C.J. Large, J. Zagari, Fabrication of microstructured polymer optical fibres, Opt. Fiber Technol. 10 (4) (2004) 325–335.

[6] S.C. Xue, R.I. Tanner, G.W. Barton, R. Lwin, M.C.J. Large, L. Poladian, Fabrication of microstructured optical fibres, Part I: Problem formulation and numerical modelling of transient draw process, J. Lightwave Technol. 23 (7) (2005) 2245–2254.

[7] S.C. Xue, R.I. Tanner, G.W. Barton, R. Lwin, M.C.J. Large, L. Poladian, Fabrication of microstructured optical fibres, Part II: Numerical modelling of steady-state draw process, J. Lightwave Technol. 23 (7) (2005) 2255–2266.

[8] S.C. Xue, M.C.J. Large, G.W. Barton, R.I. Tanner, L. Poladian, R. Lwin, The role of material properties and drawing conditions in the fabrication of microstructured optical fibres, J. Lightwave Technol. 24 (2) (2006) 853–860.

[9] I. Anteby, I. Shai, A. Arbel, Numerical calculations for combined conduction and radiation transient heat transfer in a semitransparent medium, Numer. Heat Transfer: Part A 37 (4) (2000) 359–371.

[10] M.Y. Kim, S.W. Baek, Numerical analysis of conduction, convection and radiation in a gradually expanding channel, Numer. Heat Transfer: Part A 29 (7) (1996) 725–740.

[11] J.Y. Murthy, S.R. Mathur, A finite-volume scheme for radiative heat transfer in semitransparent media, Numer. Heat Transfer: Part B 37 (1) (2000) 25–43.

[12] J. Liu, S.J. Zhang, Y.S. Chen, Advanced simulation of optical fiber drawing process, Numer. Heat Transfer: Part A 40 (5) (2001) 473–495.

[13] S.M.H. Sarvari, J.R. Howell, S.H. Mansouri, Inverse boundary design conduction–radiation problem in irregular two-dimensional domains, Numer. Heat Transfer: Part B 44 (3) (2003) 209–224.

[14] J. Blobner, R.A. Biaecki, G. Kuhn, Boundary-element solution of coupled heat conduction-radiation problems in the presence of shadow zones, Numer. Heat Transfer: Part B 39 (5) (2001) 451–478.

[15] P. Talukdar, S.C. Mishra, Transient conduction and radiation heat transfer with variable thermal conductivity, Numer. Heat Transfer: Part A 41 (8) (2002) 851–867.

[16] R. Siegel, J.R. Howell, Thermal Radiation Heat Transfer, Hemisphere Publishing Corporation, Washington, DC, 1992, Figs. 2–7 on pp. 22 & pp. 238–250.

[17] U.C. Paek, R.B. Runk, Physical behaviour of the neck-down region during furnace drawing of silica fibres, J. Appl. Phys. 49 (1978) 4417–4422.

[18] G.M. Homsy, K. Walker, Heat transfer in laser drawing of optical fibres, Glass Tech. 20 (1979) 20–26.

[19] M.R. Myers, A model for unsteady analysis of preform drawing, AIChE J. 35 (4) (1989) 592–602.

[20] K. Lyytikäinen, P. Råback, J. Ruokolainen, Numerical simulation of a specialty optical fibre drawing process, in: S. Kawano, V.V. Kudriavtsev (Eds.), Proceedings of 4th International ASME/JSME/KSME Symposium on Computational Technologies for Fluid/Thermal/Chemical/Stress Systems with Industrial Applications, American Society of Mechanical Engineers, Vancouver, BC, Canada, 2002, pp. 267–275.

[21] Z. Wei, K.-M. Lee, S.W. Tchikanda, Z. Zhou, S.-P. Hong, Effects of radiative transfer modelling on transient temperature distribution in semitransparent glass rod, Trans. ASME, J. Heat Transfer 125 (2003) 635643.

[22] K. Lyytikäinen, J. Zagari, G. Barton, J. Canning, Heat transfer within a microstructured polymer optical fibre preform, Model. Simul. Mater. Sci. Eng. 14 (2004) 1–11.

[23] G. Deflandre, Modeling the manufacturing of complex optical fibres: the case of the holey fibres, in: Proceedings of the 2nd International Colloquium, Valenciennes, France, 2002, pp. 150–156.

[24] E.M. Sparrow, R.D. Cess, Radiation Heat Transfer, Wadsworth Publishing Company, California, 1966, Figs. 2–4, pp. 50 & pp. 193.

[25] Fluent User's Manual, version 6.2, Fluent Inc. Centerra Resource Park, 10 Cavendish Court, Lebanon, NH 03766, USA, September 2003.

[26] R. Sayles and B. Caswell, A finite element analysis of the upper jet region of a fibre drawing flow filed, National Science Foundation NSF-18421/1, 1981.

[27] R. Bailey, Optical Fibre Technology Centre, personal communication.